Hindawi Publishing Corporation
Advances in Optics
Volume 2014, Article ID 813602, 9 pages
http://dx.doi.org/10.1155/2014/813602

Research Article

The Spectral Analysis of Dynamic Laser Speckle Patterns Generated by Brownian Particle Suspensions: A Stroboscopic Effect Based Filtering Technique

Dake Wang, James Ranger, and Adam Moyer

Department of Physics, Furman University, Greenville, SC 29613, USA

Correspondence should be addressed to Dake Wang; dake.wang@furman.edu

Received 17 April 2014; Revised 17 July 2014; Accepted 18 July 2014; Published 5 August 2014

Academic Editor: Chi-Wai Chow

The power spectrum of the time-varying intensity in the dynamic laser speckle patterns is determined by passing the shifted power spectrum through a low-pass filter which is implemented via the signal integration. The light intensity is modulated sinusoidally to induce the stroboscopic effect which shifts the resonant frequency component of the spectrum to 0 Hz. The homodyne dynamic laser speckles generated by the quasi-inelastic scattering of the Brownian motions in colloidal suspensions are investigated. Within the frequency range from 10 Hz to 10 kHz used in this work, the bandwidth of the Lorenztian power spectrums is shown to be inversely proportional to the particle size, which is in agreement with the prediction of the dynamic light scattering theory of diffusing particle. The spatial variation observed in the full-field power spectrum maps is caused by the nonuniform distribution of average speckle intensity and varies with the modulation frequency. However, the bandwidths measured at different locations are found to be intensity independent.

1. Introduction

The frequency spectrum of the dynamic laser speckle pattern, which fluctuates with time in response to the motions of the scattering centers, can be used to reveal the nature of the scatterer dynamics. A well-known example is the Doppler broadening of the scattered light by the Brownian motion of particles in colloidal suspensions. The frequency shifts generated by quasi-elastic light scatterings, however, are too small to be effectively detected by the traditional optical filtering method that is based on diffraction gratings, interferometers, or molecular filters. Optical mixing techniques, on the other hand, work well with the slower dynamic process which has a characteristic time longer than 10^{-6} sec [1]. Optical mixing techniques, such as photon correlation spectroscopy and laser Doppler velocimetry, have been adopted for a wide array of applications in biomedical and tissue optics [2–10].

Inasmuch as photon correlation spectroscopy and laser Doppler technique are based on the autocorrelation functions or their Fourier transforms, sufficiently fast sampling rates are needed to meet the Nyquist criterion in the frequency domain. In the context of blood flow imaging applications, a minimum frame rate of ~20 kHz is often needed to measure the flows in arterioles, and hundreds and more frames must be recorded to reach a spectral resolution of ~5 Hz [11, 12]. For full-field applications, the requirements on sampling and recording demand the use of high-speed multiple-channel detectors and substantial computing power for the subsequent data processing to recover the spectrum of the time-varying intensity recorded at each pixel. Although high-speed CMOS detectors with fast data transfer rates and the computing power needed for data processing are now available for full-field imaging applications [11–14], it is still desirable to device a more flexible technique that is capable of extracting the spectral information at frequencies of interest and does not rely as heavily on the hardware capacity.

In this work, we introduce a spectral filtering technique which utilizes low-pass filtering to extract the DC component of the power spectrum. The low-pass filtering is performed by the CMOS detector via the signal integration, which does

not separate signal light of different frequencies into different physical channels as the traditional optical filtering technique does. In order to extract non-DC frequency components, the spectrum is shifted in the frequency domain via the temporal modulation of the light intensity. The temporal modulation induces the stroboscopic effect; namely, if a cyclic motion has the same periodicity as the modulation frequency of the strobe light it will appear stationary in the recorded film sequence. In the language of spectral analysis, the spectrum of the cyclic motion is shifted to 0 Hz (i.e., it is made stationary). As will be explained in the theoretical section, our approach hinges on the calculation of the statistic variance resulted from the random phase angles of the sinusoidal modulation. It is this inherently statistic nature that sets this approach apart from the regular stroboscopic photography. Without the need of high-speed recordings, it can be implemented with regular multichannel detectors and is free from the limitation imposed the Nyquist criterion. As the modulation frequency can be chosen over a wide range, it has the potential for probing a wide range of frequency shifts in a variety of quasi-inelastic light scattering experiments. For instance, this large dynamic range makes it useful for mapping the speed and flow distributions of blood cells in circulatory and vascular systems. This method has been investigated for the time-varying speckle patterns generated by moving random phase objects using an imaging speckle setup [15]. Here, we demonstrate the working of this method for the Doppler broadening generated by Brownian particles in colloidal suspensions using a far-field backscattering configuration.

Temporal modulation technique has been applied to fluorescence lifetime imaging, where the modulation of the excitation light or the detector sensitivity is used to generate the phase delay between the fluorescence signals and the excitation [16–19]. However, the time-delay or phase-shift is not the quantities of interest in our work. A wide-field heterodyne optical mixing configuration, which also operates in frequency domain and makes use of low-frame-rate multiple-channel detectors, has been developed for imaging the Doppler signature of the cerebral blood flow [20, 21]. This scheme differs from ours in that it employs a frequency-shifted local oscillator and is derived from the off-axis holographic method which offers it a high sensitivity at the price of the reduced field of view. Recently, an intensity fluctuation modulation (IFM) method has been applied to obtain full-field laser speckle microvessel images [22]. Contrary to our approach, the IFM imaging is insensitive to flow velocity and is used to reconstruct microvessel images.

2. Theory

Instead of shifting the band-pass filter over the spectral range of interest, as in the case of most filtering techniques, we shifted the signal spectrum itself by the sinusoidal modulation of the intensity $I(t)$, producing the modulated intensity signal: $I(t, f_0, \varphi) = [1 + \Delta \cdot \cos(2\pi f_0 t + \varphi)] \cdot I(t)$, where Δ is the modulation depth which is smaller than unity, f_0 the modulation frequency, and φ the phase angle of the sinusoidal modulation at the start of each recording. In the frequency domain, the modulation gives rise to two side-bands which are located at $-f_0$ and f_0:

$$X(f, f_0, \varphi) = X(f) + \frac{1}{2}\Delta\left[e^{-i\varphi} \cdot X(f + f_0) + e^{i\varphi} \cdot X(f - f_0)\right], \quad (1)$$

where $X(f, f_0, \varphi)$ and $X(f)$ are the Fourier transforms of $I(t, f_0, \varphi)$ and $I(t)$, respectively.

In this approach, the low-pass filtering is implemented via the signal integration which yields the DC component of the time-varying signal in the limit of very long integration time. In practice, the integration time should be much longer than the decorrelation time associated with the time-varying intensity signal and the characteristic time of the modulation. The DC component of $X(f, f_0, \varphi)$, obtained via the low-pass filtering is

$$F(f_0, \varphi) = X(0) + \Delta\left[\cos\varphi \cdot X_R(f_0) + \sin\varphi \cdot X_I(f_0)\right], \quad (2)$$

where $X_R(f_0)$ and $X_I(f_0)$ are the real and imaginary parts of the spectrum $X(f)$ at the modulation frequency (i.e., the resonant frequency component), respectively.

To obtain the power spectrum, a series of $F(f_0, \varphi_n)$ are recorded at a numbers of random phase angles φ_n. It can be shown that the statistic variance in $F(f_0, \varphi_n)$ is directly proportional to the power spectrum of the intensity signal $I(t)$ [15]:

$$\mathrm{Var}\left[F(f_0, \varphi_n)\right] \propto \left|X(f_0)\right|^2, \quad (3)$$

where the power spectrum is given by: $|X(f_0)|^2 = X_R^2(f_0) + X_I^2(f_0)$. This relationship between the variance and the power spectrum can be understood by considering two situations: f_0 is close to the characteristic frequency of the time-varying signal and f_0 is very different from the characteristic frequency. In the former, any change in the phase angle will give rise to a substantial variation in $F(f_0, \varphi_n)$; that is, the frame-to-frame variance is large, whereas, in the latter, $F(f_0, \varphi_n)$ is insensitive to the phase angle and the variance is small.

To calculate the variance with high confidence, adequate numbers of recordings will be needed so that the random phase angles can go through sufficient numbers of different values. Unlike the regular stroboscopic photography where the sequence of the recordings must be kept in order to faithfully reconstruct the motion, the calculation of variance does not concern the sequence of the recording. In other words, our approach is a statistic method and is suitable for analyzing the dynamic laser speckle that is stochastic in nature.

3. Experimental

An intensity-stabilized He-Ne laser (Newport), operating at 632.8 nm, was used as the coherent light source. The intensity of the light was modulated by a Pockels cell electrooptic modulator (Leysop) driven by a sinusoidal voltage. The modulator

was biased at 50% transmission and responded linearly to the driving voltage. Before reaching the samples, the modulated light was expanded by a beam expander to a diameter of 7 mm, which ensures that the light was scattered by sufficient numbers of particles and the Gaussian statistic was applicable [1]. Monodisperse polystyrene particles (Bangs Laboratories) with size ranging from 0.17 μm to 3.11 μm were mixed with DI water to form colloidal suspensions at the room temperature. The volume concentrations ranged from 0.1% to 1%, with the lowest concentrations used for smaller particles, to ensure that the single scattering condition was met [23]. The colloidal suspensions appeared to be translucent and the Tyndall effect was clear visible.

The backscattering configuration is shown in Figure 1. The light scattered from the colloidal suspension was collected by a Fourier transform lens with a focal length of 10 cm, and the far-field speckle pattern was formed on an 8-bit 1024-by-1024 pixel CMOS sensor (Thorlabs) placed at the focal plane of the lens. The CMOS sensor was positioned with its edge aligned with the optical axis of the system to record half of the scattering pattern (because the scattering pattern is symmetric about the optical axis, this arrangement makes a better use of CMOS sensor and covers a greater range of scattering angles). An iris was placed near the lens to control the speckle size. A polarizer-analyzer pair was cross polarized to cut out the specular reflection from the cuvette. In the absence of the local oscillator, the experimental setup is expected to measure the homodyne spectrums. The integration times ranged from 100 ms to 3 s, making them much longer than the estimated characteristic times of the Brownian motion in the samples tested in our experiments.

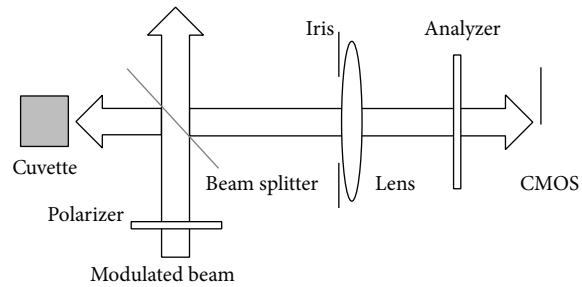

Figure 1: Schematic diagram of the backscattering configuration for recording the far-field dynamic speckle pattern. The light scattered from the colloidal suspension in the cuvette was collected by the Fourier transform lens, and the far-field speckle pattern was formed on the CMOS sensor placed at the focal plane of the lens.

4. Result and Discussion

For each type of colloidal suspensions, 102 frames of speckle patterns were recorded at each modulation frequency. Figure 2(a) shows a typical speckle patterns produced by Brownian particles with a diameter of 2.08 μm in the absence of modulation. The intensity profile is measured along the horizontal reference line in Figure 2(a) and plotted in Figure 2(b). The speckle intensity is stronger at the left edge of the field where the optical axis is located (thereafter called the center of the field) and decreases towards the edge of the field, largely a result of the vignetting effect [24]. The speckle patterns produced by smaller particles are characterized by similar patterns where the speckle intensity decreases towards the edge, albeit to a slightly lesser degree, which is most likely caused by the wider angular distribution of the light scattered by smaller particles [25]. The average speckle size was found to be about 5 times that of the pixel size, meeting the Nyquist criterion in the spatial domain [26].

In the presence of the temporal modulation, although the overall appearance of the speckle pattern remains the same, the time-integrated intensity recorded at each pixel (i.e., the DC component given in (2), obtained via low-pass filtering) fluctuates from one frame to the next. A 20-by-20 pixel region-of-interest (ROI) located at the left end of the reference line is chosen for computing the frame-to-frame variance of the speckle intensity at each modulation frequency. The 400-pixel-averaged intensity in the ROI recorded at each frame is plotted in Figure 3(a) for two time-varying intensity series, with one recorded at a modulation frequency of 10 Hz, while the other is recorded at 400 Hz. According to (3), the extent of variation is directly proportional to the power spectrum at the modulation frequency, the smaller variation observed at $f_0 = 400$ Hz (the lower curve in Figure 3(a)) can then be explained by the fact that the homodyne power spectrum deceases monotonically with increasing frequency. For the 2.08 μm particles shown in Figure 3(a), the change in the extent of the frame-to-frame variation is most obvious when the modulation frequency increases from 10 Hz to 100 Hz. As its power spectrum levels out at higher frequencies, the frame-to-frame variation no longer change appreciably with increasing modulation frequency. To the contrary, the frame-to-frame variation observed for the 0.17 μm particles remains almost constant from $f_0 = 10$ Hz to 100 Hz, indicating a much flatter power spectrum at the low end of the frequency range.

Similar to the calculation of the mean value of a stochastic variable, the frame-to-frame variance fluctuates from one calculation to the next. The accuracy of the frame-to-frame variance obviously improves with increasing number of frames used in each calculation. To find out how many frames are needed, the frame-wise variance is evaluated using increasing numbers of frames, with each calculation repeated multiple times to form a set of variance values. In other words, each set of variance values consists of multiple calculations performed using the same number of frames, and the standard deviation is computed for each set of variance values. As expected, the standard deviation of the variance in each set decreases with increasing number of frames used in the calculation. As shown in Figure 3(b), there is no significant drop in the standard deviation of the variance, once the number of frames used in calculating the variance exceeds 100 frames. Thus, it is used as the number of frames for all the calculations of variance in this work.

The power spectrum of the intensity is the Fourier transform of the intensity autocorrelation $g_2(\tau)$, whose normalized form is given by the Siegert relation as $g_2(\tau) =$

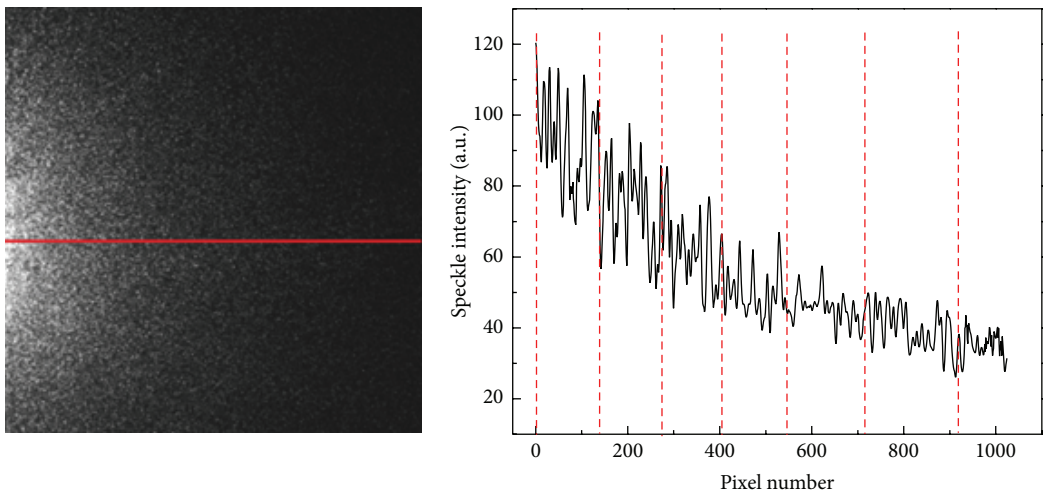

(a) (b)

Figure 2: (a) A typical laser speckle pattern (1024-by-1024 pixels) produced by the 2.08 μm particles. (b) The speckle intensity profile measured along the horizontal reference line given in Figure 2(a). The dashed vertical lines mark the locations of ROIs used for the spectral analysis.

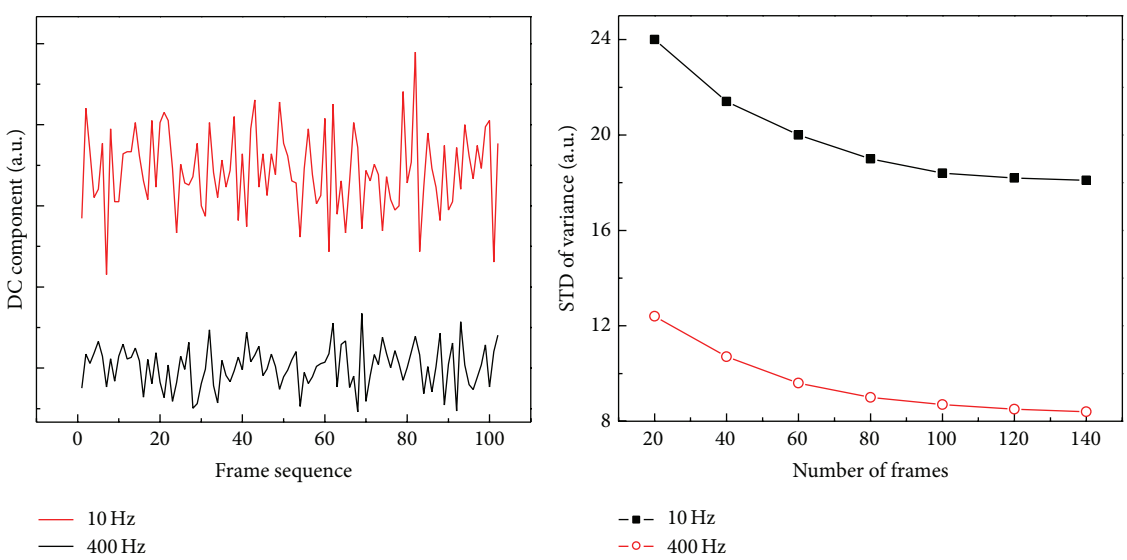

(a) (b)

Figure 3: (a) The frame-wise fluctuation of the 400-pixel-averaged intensity in the ROI located at the field center for the 2.08 μm particles at two modulation frequencies: 10 Hz and 400 Hz. (b) The standard deviation in the frame-wise variance calculated using different numbers of frames. The solid lines are guides to the eyes.

$1 + \beta|g_1(\tau)|^2$, where β is a number depending on the ratio of detector pixel size to speckle size [27, 29]. For diffusing Brownian particles, the electric field autocorrelation $g_1(\tau)$ is given by the diffusion coefficient D and the scattering wavevector q: $g_1(\tau) = \exp(-Dq^2\tau)$. The Fourier transform of $g_2(\tau) = 1 + \beta\exp(-2Dq^2\tau)$ then gives the well-known Lorentzian power spectrum. The frame-to-frame variance of the pixel-averaged intensity in the ROI is computed using 102 frames recorded at each modulation frequency, and the result is plotted against the frequency in Figure 4(a). The data points are fitted to the Lorentzian power spectrum:

$$|X(\omega)|^2 = B + \frac{C \cdot \Delta\omega}{\left[\omega^2 + \Delta\omega^2\right]}, \tag{4}$$

where the bandwidth $\Delta\omega$ is $\Delta\omega = 2Dq^2$ and ω is given by the modulation frequency. With the value of $\Delta\omega$ extracted from

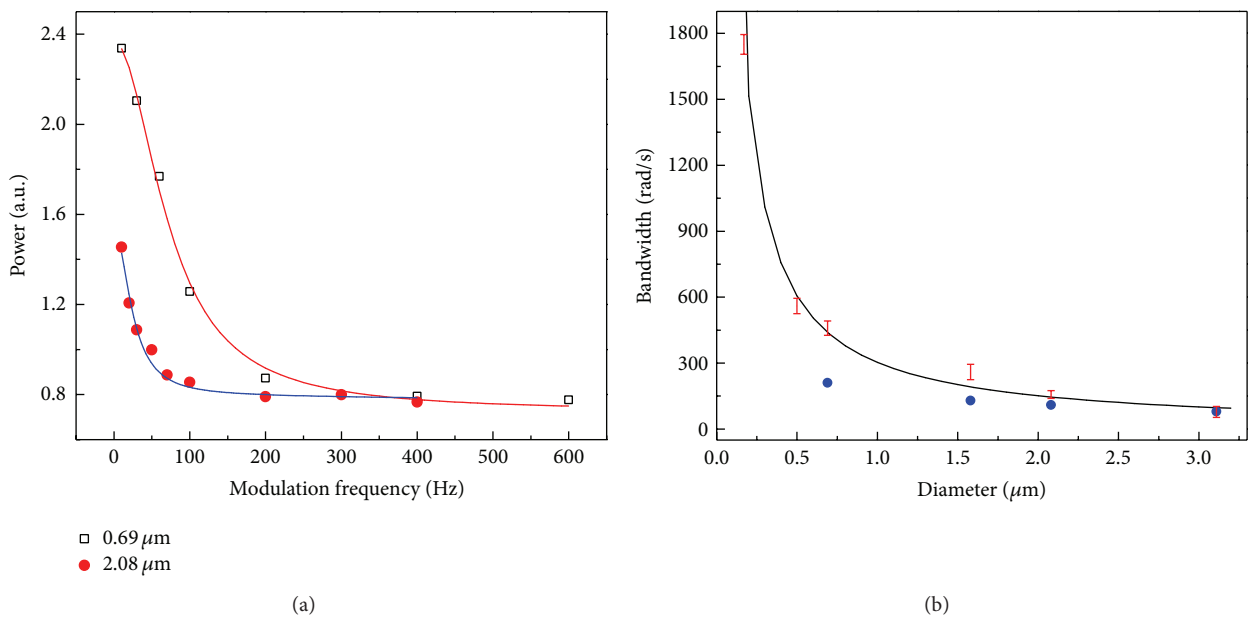

FIGURE 4: (a) The frame-wise variance of the pixel-averaged intensity in the ROI versus the modulation frequency for 0.69 μm (open squares) and 2.08 μm (solid circulars) particles. The solid lines are the Lorenztian spectral functions generated by the curve fit. (b) The bandwidths of the power spectrums obtained from the curve fit versus the actual particle diameters. The error bars are the uncertainties in $\Delta\omega$, produced by the least-square curve fitting procedure. The solid dots give the bandwidths obtained using the conventional intensity correlation analysis for dynamic speckle patterns recorded at a sampling rate of 120 Hz.

the curve fit and the scattering wavevector calculated from the 180° scattering angle, the diffusion coefficient can then be calculated. The Stokes-Einstein equation $= k_B T/6\pi\eta a$ allows the particle size, a, to be eventually determined. The $\Delta\omega$ extracted from the two sets of data points in Figure 4(a) is 152 and 459 rad/s, and the corresponding particle diameters are 1.99 μm and 0.66 μm which are in agreement with the actual particle diameters of 2.08 μm and 0.69 μm. The bandwidths of the power spectrums obtained from the curve fit are plotted against the actual particle diameters in Figure 4(b) for the colloidal suspensions tested. Comparing the six data points against the theoretical bandwidth-versus-diameter curve, which is given by the simple inverse relation, $\Delta\omega = 2k_B T q^2/6\pi\eta a$, we find that the bandwidths measured using our approach agree with the values predicted based on the single scattering assumption and the Stokes-Einstein equation.

To further demonstrate the benefit of the modulation-based filtering technique, the dynamic speckle produced by the diffusing particles was recorded using the same CMOS sensor at a frame rate of 120 fps. Each frame consists of 640-by-480 pixels, and the speckle intensity was recorded without the temporal modulation. The conventional correlation analysis was performed to analyze the speckle intensity: the intensity autocorrelation function was evaluated by performing the ensemble averaging over all pixels in each frame, and the subsequent Fourier transform yields the power spectrum. The bandwidths of the spectrums produced by different sized particles are plotted in Figure 4(b) along with the bandwidths determined by the modulation-based filtering technique. For the largest particle whose corresponding theoretical bandwidth is 97 rad/s, the 120 Hz sampling rate is adequate, and the bandwidths obtained by the two different schemes match well. As the particle size decreases and the sampling rate becomes smaller relative to the characteristic time of the intensity fluctuation, the bandwidths obtained with the conventional correlation analysis fall below the predicted values. For the smallest two particle sizes, because the power spectrums deviate substantially from the Lorenztian functional form due to the pronounced aliasing effect, the bandwidth can no longer be used to characterize the spectrums. Of course, one can trade off the number of pixels recorded in each frame for the faster frame rates. However, this tradeoff implies that one needs to use the time averaging in place of the ensemble averaging, and the advantage of multichannel detector is lost. To the contrary, in the modulation-based filtering technique, the upper bound of the measurable bandwidth is set by the modulation frequency rather than the fastest frame rate.

The values of the fitting parameter B, extracted for different particle sizes, are very close to each other, which can be verified by the observation of both fitted curves asymptotically approaching the 0.78 level in the high frequency limit in Figure 4(a). This baseline of the power spectrum presents the white noise floor, which is contributed by the sensor dark current, the amplifier readout noise, and the shot noise as well. The data recorded in dark condition reveals a negligible detector dark current; that is, the noise is intensity related. To see the dependence of the noise on the average speckle intensity, six additional ROIs, whose locations are labeled in Figure 2(b), are chosen to analyze the frame-to-frame variance and extract the fitting parameters.

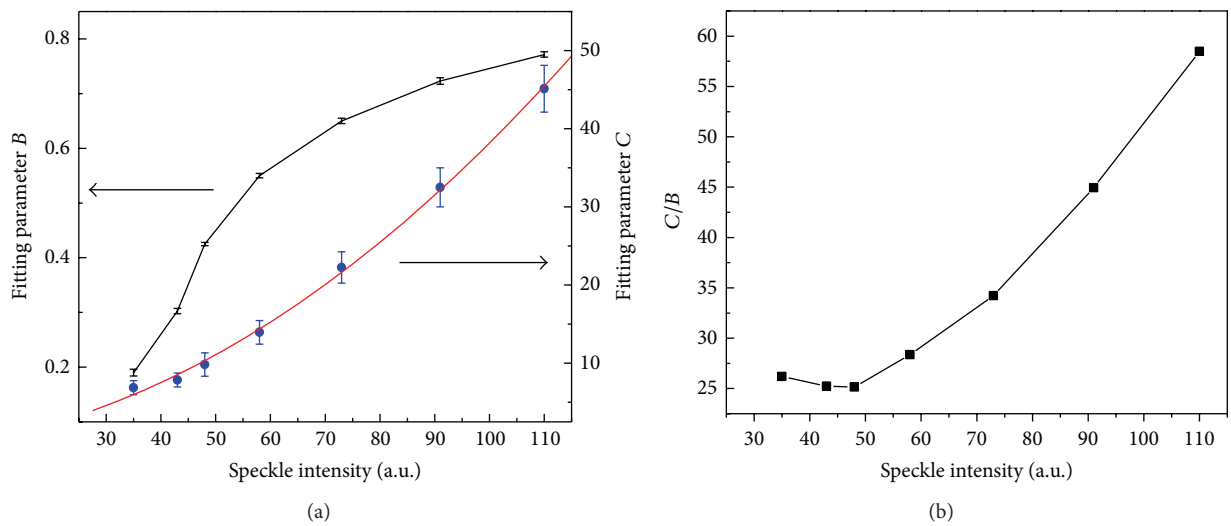

Figure 5: (a) The values of parameter B and C versus the speckle intensity averaged over the 400 pixels in each ROI. The red continuous curve is a quadratic function generated from the curve fit. The error bars are the uncertainties in B and C, produced by the least-square curve fitting of (4). (b) The ratio of C versus B. The solid line is a guide to the eyes.

As shown in Figure 5(a), the value of parameter B decreases with decreasing speckle intensity which is averaged over the 400 pixels in each ROI. In case of pure shot noise, the noise power should be linearly proportional to the average intensity. Therefore, the nonlinear nature of the intensity dependence of the noise observed in our experiment implies that it has a more complicated origin. The dependence of the other fitting parameter (parameter C in (4)) on the average intensity is also shown in Figure 5(a), and a simple quadratic relation can be seen with the help of a fitting curve. This quadratic dependence on the average intensity is an expected result based on the definition of the statistic variance. It is worth noting that although the values of parameter B and C do not affect the Lorenztian power spectrum, as shown in (4), the ratio of C/B does affect the signal-to-noise ratio which decreases with decreasing intensity.

The frame-to-frame variance of the pixel intensity for the entire field is also computed, and the results obtained at $f_0 = 10$ Hz and 400 Hz are shown in Figures 6(a) and 6(b), where the gray level at a pixel stands for the variance in the 102 intensity values recorded at this pixel. In both maps, the variance declines from the center of the filed to the edge, but the contrast in the 10 Hz map is more pronounced. The variance profiles measured along the horizontal reference lines are shown in Figures 6(c) and 6(d), which confirms the different contrast observed in Figures 6(a) and 6(b). To ensure that the less pronounced contrast observed at $f_0 = 400$ Hz is indeed related to the dynamics of the Brownian particles, the colloidal suspension was replaced by a frost glass plate which produced similar but stationary speckle patterns. The result obtained using the frost glass plate did not vary with the modulation frequency.

Given the far-filed configuration, different pixel records light scattered into different scattering angles, and consequently the variance maps are expected to show the angular distribution of the power spectrum. However, given the backscattering geometry and the small field angle (less than 5°) the change in bandwidth is merely a fraction of 1 Hz from the center of field to the edge, meaning that the bandwidth remains nearly constant across the field. Instead of being a consequence of the change in the spectrum, the contrast change observed in the variance maps is a result of both the modulation frequencies and the values of parameter C. At all field locations, the variance level, that is, the power spectrum, declines with increasing modulation frequency. But because the change in the power spectrum is amplified by parameter C, as can be seen in (4), the variance measured at the center of the field, where the values of C are greater, is more sensitive to the increasing modulation frequency. The power spectrums at $f_0 = 10$ Hz and 400 Hz are computed as functions of field locations using the fitting parameters and bandwidth obtained from the spectral analysis. The calculated power spectrums (Figures 6(c) and 6(d)) agree with the measured ones and confirm the differential declination of power spectrum from the field center to the edge. Despite the smaller contrast in the variance map observed at higher frequencies, the bandwidths measured at different ROIs show no appreciable difference as predicted. This intensity-independent feature of our approach is a great advantage in the presence of nonuniform laser source profile and artifacts caused by projecting optics. For instance, a recent study has pointed out that the spatial variations in the intensity profile can impact the flow rates measured via the laser speckle contrast imaging method [29].

5. Conclusion

We demonstrated an approach for analyzing the power spectrum of the time-varying intensity presented in dynamic laser speckle patterns. The temporal modulation of the light intensity induces the stroboscopic effect which shifts the resonant

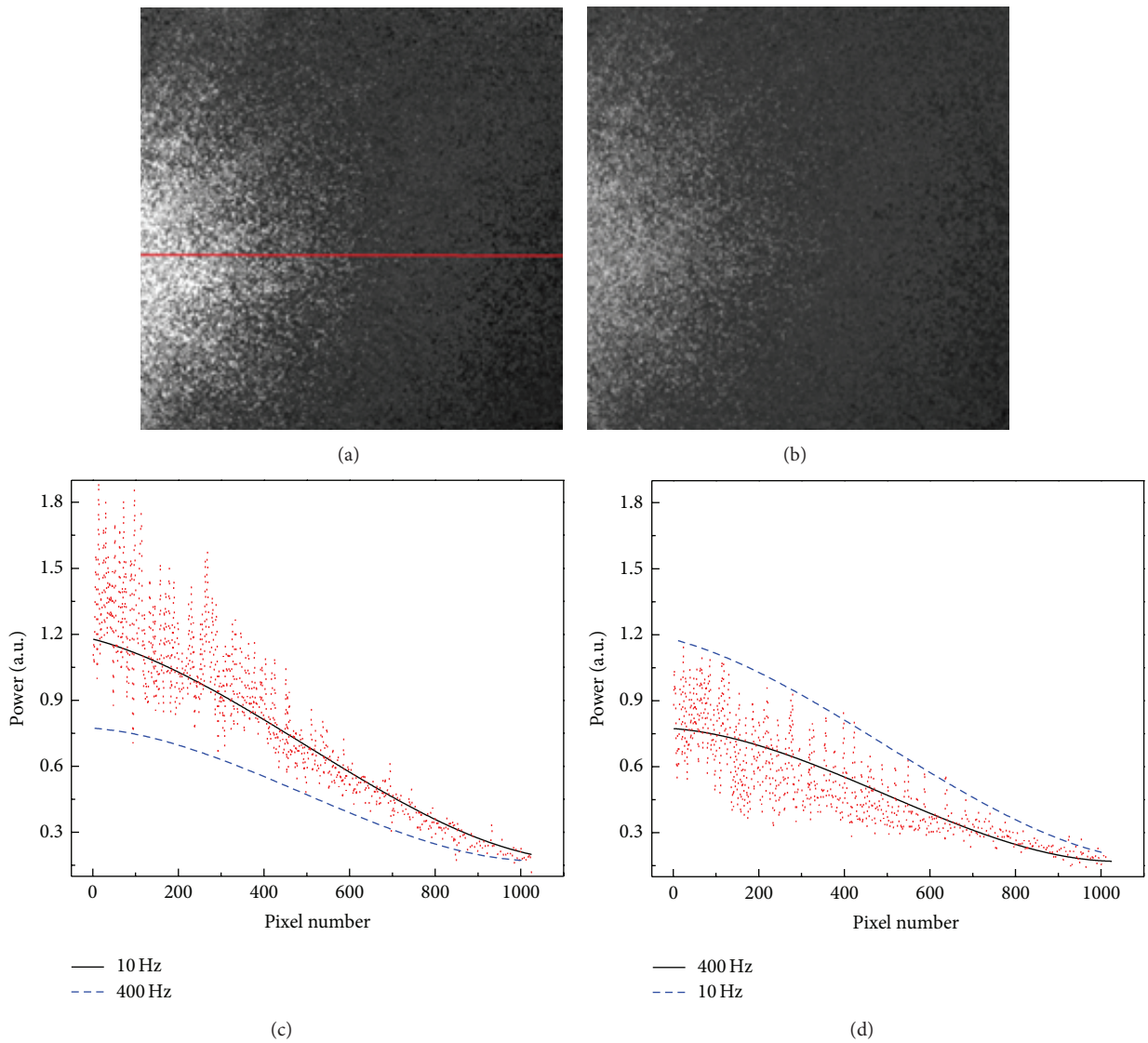

Figure 6: The full-field power spectrum maps of for 2.08 μm particles recorded at modulation frequency of 10 Hz (a), and 400 Hz (b). The power spectrum profiles (scattered dots) measured along the horizontal reference line for 10 Hz (c), and 400 Hz (d). The solid and dashed lines are the calculated power spectrum profiles at corresponding frequencies.

frequency component of the spectrum to 0 Hz. The subsequent low-pass filtering via the signal integration allows the resonant frequency component to be extracted. The random phase angle of the modulation gives rise to the frame-to-frame fluctuation which is shown to be directly proportional to the value of power spectrum at the modulation frequency.

The homodyne dynamic laser speckles generated by the quasi-inelastic scattering of the Brownian motions in colloidal suspensions are recorded at different modulation frequencies. Each frame records the DC component of the modulated spectrum, and the frame-to-frame variance yields the original power spectrum of the time-varying intensity. The frame-to-frame variance is observed to decrease with increasing modulation frequency, giving rise to the characteristic Lorenztian power spectrum produced by the Brownian particles. The diameters of the particles are obtained based on the bandwidths obtained from the spectral analysis, which is in agreement with the actual diameters. The fitting parameter extracted from the analysis indicates that the temporal noise involved in our experiments depends on the average speckle intensity in a nonlinear fashion. Both the speckle intensity patterns and the corresponding variance maps are observed to decrease from the center of the field to the edge. The level of variance drops faster with increasing modulation frequency at the field center than at the edge, reducing the contrast observed in the variance map recorded at higher frequency. This frequency dependent behavior of the full-field power spectrum distribution is satisfactorily explained by the amplifying effect of the average speckle intensity distribution across the field. The bandwidths measured at different ROIs are found to be independent of the average speckle intensity.

To determine the power spectrum over a frequency range, the modulation frequency will need to be scanned over that range. Nevertheless, the result obtained in our work demonstrates that the spectral analysis procedure can be performed with good confidence by using as few as ~10 data points for spectrums lacking complex and sharp features. Within the frequency range from 10 Hz to 10 kHz investigated in this work, the result demonstrates that the Lorenztian power spectra can be determined with a good accuracy provided that the integration time is much longer than the characteristic time of the modulation and the dynamics of scatterers. Applying this full-field temporal modulation method to study dynamics processes that generate sharp and distinct spectral bands is currently underway.

Conflict of Interests

The authors declare that there is no conflict of interests regarding the publication of this paper.

Acknowledgment

The authors would like to acknowledge the support of NSF RII South Carolina EPSCoR Program on tissue engineering (EPS-0903795).

References

[1] B. J. Berne and R. Pecora, *Dynamic Light Scattering: With Applications to Chemistry, Biology, and Physics*, Dover, New York, NY, USA, 2000.

[2] A. Humeau, J. L. Saumet, and J. P. L'Huillier, "Laser Doppler blood flowmetry multiple scattering study during reactive hyperaemia," in *Proceedings of the Optical Techniques and Instrumentation for the Measurement of Blood Composition, Structure, and Dynamics*, pp. 9–17, July 2000.

[3] K. Dörschel and G. Müller, "Velocity resolved laser Doppler blood flow measurements in skin," *Flow Measurement and Instrumentation*, vol. 7, pp. 257–264, 1996.

[4] Y. Imai and K. Tanaka, "Direct velocity sensing of flow distribution based on low-coherence interferometry," *Journal of the Optical Society of America A: Optics and Image Science, and Vision*, vol. 16, no. 8, pp. 2007–2012, 1999.

[5] F. Fitzal, D. Valentini, A. Worseg, J. Holle, and H. Redl, "Evaluation of total vs. regional blood perfusion with a laser Doppler imaging system in the rat epigastric flap," *Journal of Reconstructive Microsurgery*, vol. 17, no. 1, pp. 59–67, 2001.

[6] T. J. H. Essex and P. O. Byrne, "A laser Doppler scanner for imaging blood flow in skin," *Journal of Biomedical Engineering*, vol. 13, no. 3, pp. 189–194, 1991.

[7] W. R. Ferrell, P. V. Balint, and R. D. Sturrock, "Novel use of laser Doppler imaging for investigating epicondylitis," *Rheumatology*, vol. 39, no. 11, pp. 1214–1217, 2000.

[8] D. P. Chowdhury, C. M. Sorensen, T. W. Taylor, J. F. Merklin, and T. W. Lester, "Application of photon correlation spectroscopy to flowing Brownian motion systems," *Applied Optics*, vol. 23, no. 22, pp. 4149–4154, 1984.

[9] R. Weber and G. Schweiger, "Photon correlation spectroscopy on flowing polydisperse fluid-particle systems: Theory," *Applied Optics*, vol. 37, no. 18, pp. 4039–4050, 1998.

[10] W. V. Meyer, A. E. Smart, R. G. W. Brown, and M. A. Anisimov, "Photon correlation and scattering: introduction to the feature issue," *Applied Optics*, vol. 36, no. 30, pp. 7477–7479, 1997.

[11] A. Serov, B. Steinacher, and T. Lasser, "Full-field laser Doppler perfusion imaging and monitoring with an intelligent CMOS camera," *Optics Express*, vol. 13, p. 3681, 2005.

[12] A. Serov and T. Lasser, "High-speed laser Doppler perfusion imaging using an integrating CMOS image sensor," *Optics Express*, vol. 13, no. 17, pp. 6416–6428, 2005.

[13] M. Draijer, E. Hondebrink, T. Van Leeuwen, and W. Steenbergen, "Twente optical perfusion camera: system overview and performance for video rate laser Doppler perfusion imaging," *Optics Express*, vol. 17, no. 5, pp. 3211–3225, 2009.

[14] J. H. Park, J. Platisa, J. V. Verhagen et al., "Head-mountable high speed camera for optical neural recording," *Journal of Neuroscience Methods*, vol. 201, no. 2, pp. 290–295, 2011.

[15] D. Wang, A. Moyer, and M. Henderson, "Intensity fluctuation spectra of dynamic laser speckle patterns acquired by a full-field temporal modulation method," *Applied Optics*, vol. 51, no. 31, pp. 7576–7580, 2012.

[16] A. C. Mitchell, J. E. Wall, J. G. Murray, and C. G. Morgan, "Direct modulation of the effective sensitivity of a CCD detector: a new approach to time-resolved fluorescence imaging," *Journal of Microscopy*, vol. 206, no. 3, pp. 225–232, 2002.

[17] C. G. Morgan, Y. Hua, A. C. Mitchell, J. G. Murray, and A. D. Boardman, "A compact frequency domain fluorometer with a directly modulated deuterium light source," *Review of Scientific Instruments*, vol. 67, no. 1, pp. 41–47, 1996.

[18] J. R. Lakowicz and K. W. Berndt, "Lifetime-selective fluorescence imaging using an rf phase-sensitive camera," *Review of Scientific Instruments*, vol. 62, no. 7, pp. 1727–1734, 1991.

[19] P. Herman, B. P. Maliwal, H. Lin, and J. R. Lakowicz, "Frequency-domain fluorescence microscopy with the LED as a light source," *Journal of Microscopy*, vol. 203, no. 2, pp. 176–181, 2001.

[20] M. Simonutti, M. Paques, J. A. Sahel et al., "Holographic laser Doppler ophthalmoscopy," *Optics Letters*, vol. 35, no. 12, pp. 1941–1943, 2010.

[21] M. Atlan, M. Gross, B. C. Forget, T. Vitalis, A. Rancillac, and A. K. Dunn, "Frequency-domain wide-field laser Doppler in vivo imaging," *Optics Letters*, vol. 31, no. 18, pp. 2762–2764, 2006.

[22] Y. Zeng, M. Wang, G. Feng, X. Liang, and G. Yang, "Laser speckle imaging based on intensity fluctuation modulation," *Optics Letters*, vol. 38, no. 8, pp. 1313–1315, 2013.

[23] A. Quirantes, F. Arroyo, and J. Quirantes-Ros, "Multiple light scattering by spherical particle systems and its dependence on concentration: a T-matrix study," *Journal of Colloid and Interface Science*, vol. 240, no. 1, pp. 78–82, 2001.

[24] E. Wolf and M. Born, *Principles of Optics*, Cambridge University Press, Cambridge, UK, 7th edition, 1999.

[25] H. C. van de Hulst, *"Light Scattering by Small Particles*, Dover Publications, New York, NY, USA, 1981.

[26] D. D. Duncan, S. J. Kirkpatrick, and R. K. Wang, "Statistics of local speckle contrast," *Journal of the Optical Society of America A: Optics and Image Science, and Vision*, vol. 25, no. 1, pp. 9–15, 2008.

[27] R. Bandyopadhyay, A. S. Gittings, S. S. Suh, P. K. Dixon, and D. J. Durian, "Speckle-visibility spectroscopy: a tool to study time-varying dynamics," *Review of Scientific Instruments*, vol. 76, no. 9, Article ID 093110, 2005.

[28] T. B. Rice, S. D. Konecky, C. Owen, B. Choi, and B. J. Tromberg, "Determination of the effect of source intensity profile on speckle contrast using coherent spatial frequency domain imaging," *Biomedical Optics Express*, vol. 3, no. 6, pp. 1340–1349, 2012.

[29] P.-A. Lemieux and D. J. Durian, "Investigating non-Gaussian scattering processes by using *n*th-order intensity correlation functions," *Journal of the Optical Society of America A. Optics, Image Science, and Vision*, vol. 16, no. 7, pp. 1651–1664, 1999.